Applications and Applied Mathematics: An International Journal (AAM)

Volume 15 | Issue 2 Article 24

12-2020

Heat and Mass Transfer in Micropolar Model for Blood Flow Through a Stenotic Tapered Artery

Moses S. Dada
University of Ilorin

Funmilola Alamu-Awoniran
University of Ilorin

Available at
http://pvamu.edu/aam
Appl. Appl. Math.
ISSN: 1932-9466

Applications and Applied Mathematics:
An International Journal
(AAM)

Vol. 15, Issue 2 (December 2020), pp. 1114 – 1134

Heat and Mass Transfer in Micropolar Model for Blood Flow Through a Stenotic Tapered Artery

[1] **Moses S. Dada and** [2] **Funmilola Alamu-Awoniran**

Mathematics Department
University of Ilorin
P.M.B. 1515
Ilorin, Nigeria
[1]dadamsa@gmail.com; [2]darasimialamu@gmail.com

Received: January 31, 2019; Accepted: July 5, 2020

Abstract

Heat and mass transfer in blood flow through a tapered artery with mild stenosis is examined. The blood is considered to be an incompressible, micropolar fluid flowing through a vessel with non-symmetric axial and symmetric radial axes. The geometry of the model takes into account the shape parameter, tapered angle and height of the stenosis.The variation in the shape parameter is used to describe the changes in the axial shape of the stenosis in the artery. The governing equations for the model, comprising the continuity, momentum, energy, and mass transfer equations are transformed and simplified under the assumption of mild stenosis. Analytical solutions for the equations are obtained. The effect of different parameters on temperature, concentration, velocity, resistance, shear stress, pressure drop, Nusselt number, and Sherwood number are presented in graphical form, analysed and discussed. It is discovered that the blood temperature increases as micropolar spin parameter or the particle size increases. Also, its concentration is slowed down with an increase in the micropolar parameter or coupling number. The temperature in the converging artery is higher than that of diverging artery when compared under the same conditions.

Keywords: Heat and mass transfer; Micropolar fluid; Tapered artery; Blood flow; Stenosis; Analytical solution; Resistance to flow

MSC 2010 No.: 76A05, 80A20

1. Introduction

The basic roles of the cardiovascular system are to convey oxygen and nutrients, to eliminate waste and normalize temperature. Many cardiovascular diseases always lead to death. Over 17.8 million died of different types of various cardiovascular diseases reported by World Health Organization in 2018 as such cardiovascular disease is the number one world killer. Most of these cardiovascular diseases occurred due to restriction of blood flow in the artery when there is an excessive fatty component with abnormal intravascular growth deposited within the lumen of the artery narrowing or reshapeing the passage in the arteries, thereby causing the emergence of stenoses. Arteriosclerosis or stenoses is the constriction in the lumen of the arteries as a result of abnormal growth and unnatural increase in the arterial wall segment that appears at different positions in the arteries. The danger posed by cardiovascular diseases (angina, heart attack, myocardial infarction, cerebral stroke, and heart failure) has attracted many researchers to experimental and theoretical investigations of circulatory disorders. Studies have been carried out to explain the blood flow characteristics in the stenosed artery as evidenced by the work of Mann et al. (1938), Young (1968), Arunkumar (2015), Kumar (2015), Srinivasacharya and Madhavarao (2016), Prakash et al. (2004), and Neelam (2016). The investigations were done to understand properties of flow in the stenosed artery either by treating blood as Newtonian fluid or non-Newtonian fluid. Blood exhibits a non-Newtonian property naturally in small arteries due to a low shear rate. However, in large arteries, it behaves as a Newtonian fluid because of its high shear rate. Sanjev and Diwakar (2013) examined a mathematical model for pulsatile blood flow by considering the blood as Non-Newtonian power-law fluid. Sarivastava (1985) studied the effect of stenoses on the blood flow in the artery using a couple of stress fluid model.

A lot of researchers have modeled blood as micropolar fluid for its great advantages. The micropolar fluid (blood) considers fluid particle through an independent kinetic vector called a micropolar vector. A micropolar fluid is a fluid in which microelements of the fluid are considered to be rigid (Agarwal et al. (1987), Philip et al. (1995) and Prakash et al. (2015)). Erigen (1966) brought about the concept of micropolar fluid particles to generalized concentrated suspension of neutrally buoyant damaged particles in a viscous fluid. Many investigations have been carried out on blood flow in a stenosed artery by taking the blood to be micropolar fluid. Bhavana et al. (2016) investigated a mathematical model for mild stenosis, micropolar fluid flow through an artery with the effect of stenosis, and post stenotic dilation. He found out that the resistance to flow and wall shear stress increased with the height of stenosis. Ariam (1974) investigated blood flow in arteries taking it as a rigid circular tube and concluded that it was better to model blood in a micropolar fluid because it accounted for the micro-rotation of blood suspension.

Naturally, the shape of the arteries is tapered. Mekheimer (2008) investigated the flow of blood in a tapered artery in the presence of mild stenoses in a micropolar fluid. Ranama and Srikamath (2015) worked on blood flow through an overlapping clogged tapered artery in the presence of cather under the assumption of mild stenosis. Kumar and Diwakar (2013) studied the effects of multiple stenoses and post stenotic dilation, treating blood as Bingham plastic fluid and observed that an increase in yield stress decreases the blood viscosity. Mir Golam et al. (2013) developed a model on pulsatile non-Newtonian blood flow through arterial stenosis. It was discovered that there is a

sudden increase in stress at the center of stenosis. Arun Kumar (2016) developed a mathematical model on blood flow under the atherosclerosis condition. It was observed that resistance to flow decreases as the stenosis shape parameter increase but decreases as the size of stenosis increases. The above studies, though facilitating, considered the flow of blood in a stenosed artery without accounting for the heat and mass transfer of the blood flow.

The importance of heat transfer on the flow in a blood vessel has led some researchers to study the effects of heat transfer in the blood (Makinde et al. (2017), Charm et al. (1968), Chaiyoka and Makinde (2014)). Also, Ogulu and Abbey (2005) examined the effect of heat transfer on the motion of blood in a stenosed or disease artery under the optically thin fluid. Chakvarty and Sen (2005) described the dynamic response of heat and mass transfer in blood flow in bifurcated arteries under the influence of stenosis. Moreover, the amount and nature of heat transfer in a biological system (human being) can be known using an external magnetic field. Consequently, Nadeem et al. (2011) investigated the influence of heat and mass transfer on Newtonian Biomagnetic fluid on blood flow through a tapered porous artery with mild stenoses but not as micropolar fluid flow. Abubakar and Adeoye (2020) investigated the influence of radiative heat and magnetic field on blood flow in an inclined tapered stenosed artery.

Although the above studies on heat transfer in blood flow are impressive, however, there is a dearth of knowledge on combined effects of heat and mass transfer in micropolar blood flow with stenoses in a tapered artery. Hence, this paper examines the effects of heat and mass transfer in a micropolar fluid model for blood flow through a tapered artery with stenosis.

2. Mathematical formulation

Let (r, θ, x) be the cylindrical polar co-ordinates with $r = 0$ as the axis of symmetry of the tube. The flow considered is incompressible micropolar fluid with constant viscosity μ and density ρ in the tube of length L. w_x and w_r are radial and axial velocity components respectively. Let the radius of the tapered stenotic artery at point x be expressed as

$$h(x) = \begin{cases} r(x)\left[1 - \eta(a_2^{n-1}(x - a_1) - (x - a_1)^n\right], & a_1 \leq x \leq a_1 + a_2, \\ r(x), & \text{otherwise}, \end{cases} \tag{1}$$

with

$$r(x) = r_0 + \xi x, \tag{2}$$

where r_0 and $r(x)$ are the radii of the non tapered artery and tapered arterial segment in the non stenotic region, respectively, ξ is the tapered angle ($\xi = \tan\phi$), for converging ($\xi \leq 0$), diverging ($\xi \geq 0$) and non- tapered angle $\xi = 0$. a_2 is the length of the stenosis , ($n \geq 2$) is the shape parameter determining the shape of the constriction region which is symmetric at $n = 2$ and

$$\eta = \frac{\delta n^{n|n-1}}{r_0 a_2^n (n-1)}, \tag{3}$$

where δ denote the maximum height of the stenosis located at

$$x = a_1 + \frac{a_2}{n^{n|(n-1)}}. \tag{4}$$

The geometry of the stenosis is described in Figures 1 and 2 below.

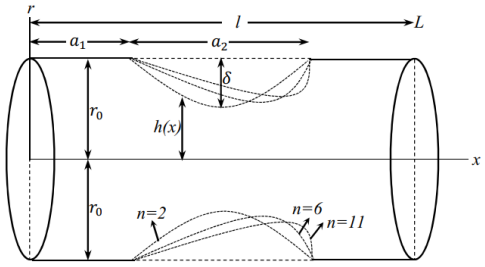

Figure 1. The geometry of the tapered artery

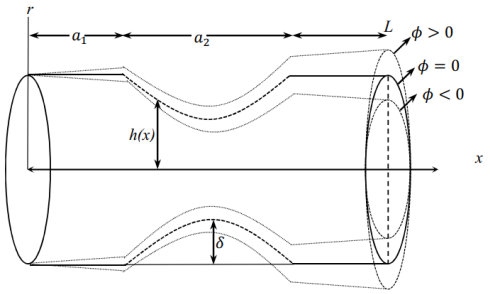

Figure 2. Geometry of arterial segment under consideration for different tapered angles

The governing equations for the steady flow of an incompressible micropolar fluid in the absence of body and couple forces may be expressed as follows:

$$\nabla.\mathbf{w} = 0, \tag{5}$$

$$\rho(\mathbf{w}.\nabla\mathbf{w}) = -\nabla\mathbf{p} + k\nabla\times\mathbf{w} + (\mu+k)\nabla^2\mathbf{w}, \tag{6}$$

$$\rho j(\mathbf{u}.\nabla\mathbf{u}) = -2k\mathbf{u} + k\nabla\times\mathbf{w} - \gamma(\nabla\times\nabla\times\mathbf{w}) + (\alpha+\beta+\gamma)\nabla(\nabla.\mathbf{u}), \tag{7}$$

$$\rho c_p(\mathbf{T}\cdot\nabla\mathbf{T}) = k\nabla^2\mathbf{T} + \mathbf{S}.L, \tag{8}$$

and

$$(\mathbf{C}\cdot\nabla\mathbf{C}) = D\nabla^2\mathbf{C} + \frac{Dk_T}{T_m}\nabla^2\mathbf{T}, \tag{9}$$

where

$$\mathbf{S} = -\rho I + \mu B_1, B_1 = L + L^1, \tag{10}$$

where L is the gradient of vector $\mathbf{w}$, $\mathbf{p}$ is the fluid pressure, $\mathbf{u}$ is the micro rotation vector, j is the microgyration parameter, c_p is the specific heat at constant pressure, T_m is temperature of the medium, D is the coefficients of mass diffusivity, k_T is the thermal diffusion ratio, k denotes the thermal conductivity and C is the concentration of the fluid. μ, k' are coefficients of shear and vortex

viscosity respectively. γ , β, α are respectively coefficients of viscosities. The material constants μ, k', α, β and γ satisfy the following inequalities (Eringen 1966),

$$2\mu + k' \geq 0, \quad k' \geq 0, \quad 3\alpha + \beta + \gamma \geq 0 \quad \gamma \geq |\beta|. \tag{11}$$

The flow is axis symmetric and the velocity vector for the flow is expressed by $\mathbf{w} = (w_r, 0, w_x)$ where w_r, w_x are velocities in r and x directions, respectively. Fluids with microstructure has the ability to rotate independently of the fluid movement (Gregorz Lukaseicz(1999)). Hence, the micro rotation vector $\mathbf{u}$ is expressed as $\mathbf{u} = (0, \varpi, 0)$. The model governing equations becomes

$$\frac{\partial w_r}{\partial r} + \frac{w_r}{r} + \frac{\partial w_x}{\partial x} = 0, \tag{12}$$

$$\rho\left[w_r\frac{\partial w_x}{\partial r} + w_x\frac{\partial w_x}{\partial x}\right] = -\frac{\partial p}{\partial x} + (\mu + k')\left[\frac{\partial^2 w_x}{\partial r^2} + \frac{1}{r}\frac{\partial w_x}{\partial r} + \frac{\partial^2 w_x}{\partial x^2}\right] + \frac{k'}{r}\frac{\partial(r\varpi)}{\partial r}, \tag{13}$$

$$\rho\left[w_r\frac{\partial w_r}{\partial r} + w_x\frac{\partial w_r}{\partial x}\right] = -\frac{\partial p}{\partial r} + (\mu + k)\left[\frac{\partial^2 w_r}{\partial r^2} + \frac{1}{r}\frac{\partial w_r}{\partial r} - \frac{w_r}{r^2}\right] - k\frac{\partial(\varpi)}{\partial x}, \tag{14}$$

$$\rho j\left(w_r\frac{\partial \varpi}{\partial r} + w_x\frac{\partial \varpi}{\partial x}\right) = -2k\varpi - k\left(\frac{\partial w_x}{\partial r} - \frac{\partial w_r}{\partial x}\right) + \gamma\left(\frac{\partial}{\partial r}\left(\frac{1}{r}\frac{\partial(r\varpi)}{\partial r}\right) + \frac{\partial^2 \varpi}{\partial x^2}\right), \tag{15}$$

$$\rho c_p\left[w_r\frac{\partial T}{\partial r} + w_x\frac{\partial T}{\partial x}\right] = k'\left[\frac{\partial^2 T}{\partial r^2} + \frac{\partial T}{\partial r}\right] + (\mu + k)\left[\frac{\partial w_x}{\partial r}\right]^2, \tag{16}$$

and

$$\left(w_r\frac{\partial C}{\partial r} + w_x\frac{\partial C}{\partial x}\right) = D\left(\frac{\partial^2 C}{\partial r^2} + \frac{1}{r}\frac{\partial C}{\partial r} + \frac{\partial^2 C}{\partial x^2}\right) = \frac{Dk_T}{T_m}\left(\frac{\partial^2 T}{\partial r^2} + \frac{1}{r}\frac{\partial T}{\partial r} + \frac{\partial^2 T}{\partial x^2}\right), \tag{17}$$

with the following boundary conditions

$$\frac{\partial w_x}{\partial r} = 0 \quad \text{at} \quad r = 0, \tag{18}$$

$$w_x = 0 \quad \text{at} \quad r = h(x), \tag{19}$$

$$\varpi = 0 \quad \text{at} \quad r = h, \tag{20}$$

$$\varpi, w_x \quad \text{are finite at} \quad r = 0, \tag{21}$$

$$\frac{\partial \theta}{\partial r} = 0 \quad \text{at} \quad r = 0, \tag{22}$$

$$\frac{\partial \sigma}{\partial r} = 0, \quad \text{at} \quad r = 0, \tag{23}$$

and

$$\sigma = 0, \theta = 0 \quad \text{at} \quad r = h(x). \tag{24}$$

Introducing the following non dimensional variables

$$\left.\begin{aligned} x' &= \frac{x}{a_2}, \quad \delta' = \frac{\delta}{r_0}, \quad r' = \frac{r}{r_0}, \quad p' = \frac{p}{\frac{\mu\varpi a_2}{r_0^2}}, \\ \xi' &= \frac{\xi' a_2}{r_0}, \quad \gamma_1 = \frac{a_1}{a_2}, \quad h = \frac{h'}{r_0}, \\ w_x' &= \frac{w_x}{\omega}, \quad w_r' = \frac{a_2 w_r}{\omega\delta}, \\ \varpi' &= \frac{r_0\varpi}{\omega}, \quad \delta' = \frac{\delta}{r_0}, \\ \theta &= \frac{T - T_1}{T_w - T_1}, \quad Ec = \frac{w_x^2}{c_p(T_w - T_1)}, \quad P_r = \frac{\mu c_p}{k}, \\ \sigma &= \frac{C - C_1}{C_w - C_1}, \quad Sc = \frac{\nu}{D}, and \\ S_r &= \frac{DK_T}{\nu T_m}\frac{(T_w - T_1)}{(C_w - C_1)}. \end{aligned}\right\} \tag{25}$$

The average velocity over section of the tube of the width r_0 is ω. Making use of dimensionless variables (25) and after implementing the additional following conditions (Mekheimer and Elkot 2008),

$$(i) \qquad Re\frac{\delta n^{\frac{1}{(n-1)}}}{b} << 1, \tag{26}$$

$$(ii) \qquad \frac{r_0 n^{\frac{1}{(n-1)}}}{b} \approx (1), \tag{27}$$

Equation (1) describing the geometry of the stenosis in the artery is

$$h(x) = \begin{cases} \left[(1-\xi x)(1 - \eta_1(x-\gamma_1) - (x-\gamma_1)^n\right], & \gamma_1 \le x \le \gamma_1 + 1, \\ 1 + \xi x', & \text{otherwise}, \end{cases} \tag{28}$$

where

$$\eta_1 = \frac{\delta' n^{\frac{n}{(n-1)}}}{n-1}. \tag{29}$$

Dropping the prime on dimensionless variables, Equations (12) - (17) for the case of mild ($\frac{\delta}{r_0} << 1$) reduce to

$$\frac{\partial w_x}{\partial r} = 0, \tag{30}$$

$$\frac{\partial p}{\partial r} = 0, \tag{31}$$

$$\frac{\partial p}{\partial x} = \frac{1}{1-N}\left(\frac{\partial^2 w_x}{\partial r^2} + \frac{1}{r}\frac{\partial w_x}{\partial r} + \frac{N}{r}\frac{\partial(r\varpi)}{\partial r}\right), \tag{32}$$

$$2\varpi = -\frac{\partial w_x}{\partial r} + \frac{2-N}{m^2}\frac{\partial}{\partial r}\left(\frac{1}{r}\frac{\partial(r\varpi)}{\partial r}\right), \tag{33}$$

$$\frac{\partial^2\theta}{\partial r^2} + \frac{1}{r}\frac{\partial\theta}{\partial r} + Br(K_1 + 1)\left(\frac{\partial w_x}{\partial r}\right)^2 = 0, \tag{34}$$

$$\frac{1}{Sc}\left[\frac{1}{r}\frac{\partial\sigma}{\partial r}+\frac{\partial^2\sigma}{\partial r^2}\right]+Sr\left[\frac{1}{r}\frac{\partial\theta}{\partial r}+\frac{\partial^2\theta}{\partial r^2}\right]=0, \tag{35}$$

where $N=\dfrac{k'}{\mu+k'}, (0\leq N\leq 1)$ is coupling number, $Br=EcP_r$,

$$m^2=\frac{r_0^2k'(2\mu+k')}{\gamma(\mu+k')}, \tag{36}$$

is the micropolar parameter, Sc is the Schmidt number, Sr is the Soret number,

$$K_1=\frac{k}{\mu}, \tag{37}$$

where $K_1$is the micropolar or material parameter.

The corresponding non dimensional boundary conditions are

$$\frac{\partial w_x}{\partial r}=0 \quad \text{at} \quad r=0, \tag{38}$$

$$w_x=0 \quad \text{at} \quad r=h(x), \tag{39}$$

$$\varpi=0 \quad \text{at} \quad r=h, \tag{40}$$

$$\varpi, w_x \quad \text{are finite at} \quad r=0, \tag{41}$$

$$\frac{\partial\theta}{\partial r}=0 \quad \text{at} \quad r=0, \tag{42}$$

$$\frac{\partial\sigma}{\partial r}=0, \quad \text{at} \quad r=0, \tag{43}$$

$$\sigma=0, \theta=0 \quad \text{at} \quad r=h(x). \tag{44}$$

3. Problem solution

Equation (32) can be rewritten as

$$\frac{\partial}{\partial r}\left(r\frac{\partial w_x}{\partial r}+Nr\varpi-(1-N)\frac{r^2}{2}\frac{\partial p}{\partial x}\right)=0. \tag{45}$$

Integrating Equation (45) to get

$$\frac{\partial w_x}{\partial r}=-N\varpi+(1-N)\frac{r}{2}\frac{\partial p}{\partial x}+\frac{c_1(x)}{r}, \tag{46}$$

From Equations (46) and (33), we have

$$\frac{1}{m^2}\frac{\partial^2\varpi}{\partial r^2}+\frac{1}{rm^2}\frac{\partial\varpi}{\partial r}-\left(\frac{1}{r^2m^2}+1\right)\varpi=\frac{(1-N)}{4-2N}\left\{\frac{r}{2}\frac{\partial p}{\partial x}+\frac{c_1(x)}{r}\right\}. \tag{47}$$

The general solution of Equation (47) is

$$\varpi=C_2(x)I_1(mr)+C_3(x)K_1(mr)-\frac{(1-N)}{4-2N}\left\{r\frac{\partial p}{\partial x}\right\}, \tag{48}$$

where $I_1(mr)$ and $K_1(mr)$ are modified first order Bessel function of first and second kind, respectively. Substituting Equation (48) into Equation (46) and integrate with respect to r to obtain

$$w_x = \frac{(1-N)}{(4-2N)} r^2 \frac{\partial p}{\partial x} - \frac{N}{m}[c_2(x) I_0(mr) + c_3(x) K_0(mr)] + c_4(x), \tag{49}$$

where $I_0(mr)$ and $K_0(mr)$ are modified zero order Bessel function of first and second kind, respectively, and $c_4(x)$ is the constant of integration. Based on the definition of $K_0(mr)$, the arbitrary function c_3=0 for ϖ, w_x must be finite on $r = 0$. The remaining arbitrary functions in Equations (48) and (49) are determined using the boundary conditions (39) and (40). Hence,

$$c_2(x) = \frac{\frac{(1-N)}{(2-N)} \frac{h}{2} \frac{\partial p}{\partial x}}{I_1(mh)}, \tag{50}$$

$$c_4(x) \;=\; \frac{\frac{N}{m}\left[\left(\frac{1-N}{2-N}\right)\frac{h}{2}\,\frac{\partial P}{\partial X}\right]\, I_0(mh)}{I_1(mh)} - \frac{(1-N)}{(2-N)}\,\frac{\partial p}{\partial x}\left(\frac{h^2}{2}\right), \tag{51}$$

and

$$w_x = \chi\left\{r^2 - h^2 + \frac{Nh}{mI_1(mh)}[I_0(mh) - I_0(mr)]\right\}, \tag{52}$$

where

$$\chi = \frac{(2-N)}{(4-N)} \frac{\partial p}{dx}. \tag{53}$$

The corresponding stream function is obtained by using

$$\psi = \int r w_x dx. \tag{54}$$

Therefore,

$$\psi = -\chi \frac{\partial p}{dx}\left\{\frac{2h^2r^2 - r^4}{4} - \frac{Nh}{mI_1(mh)}[\frac{r^2 mI_0(mh) - 2rI_1(mr)}{2m}]\right\}. \tag{55}$$

Substituting the derivative of w_x in Equation (52) into Equation (34) to obtain

$$\frac{\partial^2 \theta}{\partial r^2} + \frac{1}{r^2}\frac{\partial \theta}{\partial r} = g(r), \tag{56}$$

where

$$g(r) = -Br(1+K_1)\left\{\frac{(1-N)^2}{(4-2N)^2}\left(\frac{\partial p}{\partial x}\right)^2\left[4r^2 + \frac{4rNhI_1(mr)}{I_1(mh)} + \frac{N^2h^2[I_1(mr)]^2}{[I_1(mh)]^2}\right]\right\}, \tag{57}$$

Integrating Equation (56) with respect to r, we have

$$\frac{\partial \theta}{\partial r} = \zeta\left(r^3 + \frac{f_{01}}{I_1(mh)m^2} + \frac{f_{12}}{2\left(I_1(mh)\right)^2} + \frac{C_5(r)}{r}\right), \tag{58}$$

where

$$f_{01} = 4Nh\left(I_0(mr)mr - 2\,I_1(mr)\right),$$

$$f_{12} = N^2h^2r\left(\left(I_1(mr)\right)^2 - I_0(mr)\,I_2(mr)\right),$$

and

$$\zeta = -Br(1+K_1)\frac{(1-N)^2}{(4-2N)^2}\left(\frac{\partial p}{\partial x}\right)^2. \tag{59}$$

Applying the boundary conditions on Equation (58) and with $C_5(r) \neq 0$, the expression in RHS will be undefined. Therefore, $C_5(r) = 0$ and

$$\frac{\partial \theta}{\partial r} = \zeta\left(r^3 + \frac{f_{01}}{I_1(mh)m^2} + \frac{f_{12}}{2\left(I_1(mh)\right)^2}\right). \tag{60}$$

Integrating Equation (60) and applying the boundary condition (44) to obtain

$$\theta(r) = \zeta(1/4\, r^4 + G_1(r) - G_2(r) + G_3(r) + G_4(r) - G_5(r) + G_6(r),$$

where

$$G_1(r) = \frac{4\,NrI_1(mr)hm + 8\,NI_0(mr)h}{m^3 I_1(mh)},$$

$$G_2(r) = \frac{N^2h^2m^2r^4{}_3\mathrm{F}_4(3/2,2,2;\,1,3,3,3;\,-m^2r^2)}{64\,\left(I_1(mh)\right)^2},$$

$$G_3(r) = \frac{N^2h^2\left(\sqrt{\pi}r^2m^2\left(I_0(mr)\right)^2 - 2\sqrt{\pi}rmI_0(mr)I_1(mr) + \sqrt{\pi}r^2m^2\left(I_1(mr)\right)^2\right)}{4\,m^2\sqrt{\pi}\left(I_1(mh)\right)^2},$$

$$G_4(r) = \frac{1}{4}h^4 + \frac{4\,Nh^2mI_1(mh) + 8\,NI_0(mh)}{m^3 I_1(mh)},$$

$$G_5(r) = \frac{N^2h^6m^2{}_3\mathrm{F}_4(3/2,2,2;\,1,3,3,3;\,-m^2h^2)}{64\,\left(I_1(mh)\right)^2},$$

$$G_6(r) = \frac{N^2h^2\left(\sqrt{\pi}h^2m^2\left(I_0(mh)\right)^2 - 2\sqrt{\pi}hmI_0(mh)I_1(mh) + \sqrt{\pi}h^2m^2\left(I_1(mh)\right)^2\right)}{4m^2\sqrt{\pi}\left(I_1(mh)\right)^2},$$

where ${}_3F_4(3/2,2,2;\,1,3,3,3;\,-m^2r^2)$ is hyper-geometry functions and $I_i(mh)$ is a Bessel function of order i.

Nusselt number (Nu) is calculated using

$$Nu = \left.\frac{\partial \theta}{\partial r}\right|_{r=h}. \tag{61}$$

Equation (35) may be written as

$$\frac{1}{Sc}\left[\frac{1}{r}\frac{\partial}{\partial r}\left(r\frac{\partial \sigma}{\partial r}\right)\right] = \frac{-1}{Sr}\left[\frac{1}{r}\frac{\partial}{\partial r}\left(\frac{r\partial \theta}{\partial r}\right)\right]. \tag{62}$$

Substituting Equation (58) into Equation (62), it becomes

$$\frac{\partial \sigma}{\partial r} = \frac{Sc}{Sr}\zeta\left(r^3 - \frac{f_{01}}{m^2 I_1(mh)} + \frac{f_{12}}{2\left(I_1(mh)\right)^2}\right). \tag{63}$$

Solving Equation (63) using the boundary condition (44), we have

$$\sigma(r) = \zeta\frac{Sc}{Sr}\left(1/4\, r^4 + G_1(r) - G_2(r) + G_3(r) + G_4(r) - G_5(r) + G_6(r)\right).$$

The Sherwood number at $r = h$ is calculated as follows

$$Sh = \frac{\partial \sigma(r)}{\partial r}|_{r=h}. \tag{64}$$

The volumetric flow rate is defined by

$$Q = \int_0^h r w_x dr. \tag{65}$$

Therefore,

$$Q = \left(\frac{1-N}{2-N}\right)\frac{\partial p}{\partial x}\left(\frac{-h^4}{4} + \frac{Nh^2 I_0(mr)}{2mI_1(mh)} - \frac{Nh^2}{m^2}\right). \tag{66}$$

It implies that

$$\frac{\partial p}{\partial x} = \frac{Q}{(\frac{1-N}{2-N})\left(\frac{-h^4}{4} + \frac{Nh^2 I_0(mr)}{2mI_1(mh)} - \frac{Nh^2}{m^2}\right)}. \tag{67}$$

As the micropolar fluid parameter $N \to 0$, the fluid becomes Newtonian fluid.

The pressure drop Δp across the stenotic artery from $x = 0$ to $x = L$ is

$$\Delta p = \int_0^L \left(\frac{-\partial p}{\partial x}\right) dx = 8Q \int_0^L T'(x) dx, \tag{68}$$

where

$$T'(x) = \frac{2(2-N)m^2 I_1(mh)}{(1-N)[h^2[h^2 m^2 I_1(mh) - 2mNI_0(mh) + 4I_1(mh)]]}. \tag{69}$$

So, the resistance impedance is

$$\lambda = 8\left[(L-b)J + \int_a^{a+b} T'(x) dx\right], \tag{70}$$

where

$$J = \frac{(2-N)m^2 I_1(m)}{(1-N)[m^2 I_1(m) - 2mNI_0(m) + 4I_1(m)]}. \tag{71}$$

Let

$$\bar{\lambda} = \frac{\lambda}{\lambda_0}, \tag{72}$$

where $\lambda_0 = 3L$.

Therefore,

$$\bar{\lambda} = \frac{8}{3L}(L-b)J + \frac{8}{3L}\int_a^{a+b} T'(x) dx. \tag{73}$$

The stress tensor is not symmetric for micropolar fluid, therefore, the non dimensionless wall shear stress is given by

$$\tau_{xr} = \left(\frac{\partial w_x}{\partial r} - \frac{N}{(1-N}\varpi\right), \tag{74}$$

$$\tau_{rx} = \frac{-1}{(1-N)}\left(\frac{\partial p}{\partial x} + N\varpi\right), \tag{75}$$

$$\tau_{rx} = \frac{-1}{2}(1-N)\frac{\partial p}{\partial x}h, \tag{76}$$

using Equation (46) with the boundary conditions (38) and (40).

Hence,

$$\frac{\partial w_x}{\partial r}\bigg|_{r=h} = \frac{-1}{2}(1-N)\frac{\partial p}{\partial x}h\ . \tag{77}$$

The shearing stress has its maximum height at the throat which is located at

$$x = \frac{a_1}{a_2} + \frac{1}{n^{1|(n-1)}}. \tag{78}$$

It implies that

$$\tau_s = \tau_{rx}|_{h=1-\delta}\ , \tag{79}$$

$$\tau_s = 4Q(1-\delta)I, \tag{80}$$

where τ_s is wall shear at the throat and I is defined by

$$I = \frac{(2-N)m^2 I_1(m\delta_1)}{(1-N)[(\delta_1)^2 m^2 I_1(m\delta_1) - 2mNI_0(m\delta_1) + 4I_1(m\delta_1)]}. \tag{81}$$

where δ_1=$1-\delta$.

Therefore,

$$\bar{\tau_{rx}} = \frac{(2-N)m^2 I_1(mh)}{(1-N)[h^2 m^2 I_1(mh) - 2mNI_0(mh) + 4I_1(mh)]}, \tag{82}$$

where

$$\bar{\tau_s} = \frac{\tau_s}{\tau_0}, \bar{\tau_{rx}} = \frac{\tau_{rx}}{\tau_0}, \bar{\tau_{rx}} = \tau, \tau_0 = 4Q, \tag{83}$$

with τ_0 as the wall shear stress for a flow in normal artery.

4. Results and discussion

Numerical evaluation of the analytical expression for dimensionless concentration (σ), temperature (θ), pressure drop (Δp), Nusselt number (Nu), Sherwood (Sh), velocity (w_x), shear stress or skin friction (τ), resistance to flow for non tapered, diverging tapering, and converging tapering arteries were presented using Maple 18 software in this section. The effect of different parameters such as micropolar spinning parameter (m), coupling number (N), shape parameter(n), Soret number (Sr), and Brickmann number (Br) were discussed for different fluid flow properties displayed at the Appendix in Figures 3-27.

Figures 3-4 show the effects of m (micropolar spin parameter) and N (particles size parameter) on axial velocity profile. The effects of convergence, divergence and non tapering on axial velocity are presented. It is observed that as m increases, axial velocity increases while as N increases, there is reduction in axial velocity. Axial velocity is higher in a diverging artery than converging artery.

Figures 5-6 show the resistance against δ with variation of ξ and L. It is shown that the resistance to flow or impedance is higher in a converging artery than diverging artery at the symmetric stenoses $(n = 2)$. It is observed that the greater the length of the tube, the lower the resistance to flow.

Figures 7-8 depict the wall shear stress against x with variation of ξ and m. It shows that the wall shear stress distribution increases in the diverging region than the converging region at $n = 2$. Also, it reveals that as microplolar parameter increases, there is an increase in wall shear stress.

Figures 9-13 show the temperature profile against ξ, K_1, N, m, and B_r. It is discovered that the blood temperature increases as micropolar spinning parameter or coupling number increases. The temperature in the converging artery is higher than that of diverging artery when compared under the same conditions. An increase in Brikmann number causes an increase in temperature. It is observed that temperature increases with an increase in K_1.

Figures 14-19 show the variation in concentration against r varying N, ξ, B_r, Sr, and m. It is evident from the figures that an increase in micropolar parameter or coupling number decreases concentration. Concentration is higher in a diverging artery than converging artery at $n = 2$. Hence, the concentration profile shows that as material parameters, Brikmann number or Soret number increases, concentration decreases.

Figures 20-21 show the variation in Nusselt number Nu against Br and K. It is noticed that a rise in N, decreases Nusselt number. Also, it is observed that as the value of Br increases, there is an increase in Nu. Figures 22-23 show the graph of Sherwood number against x, it is noted that as Sr or Br increases, there is an increase in Sherwood number, Sh. Figures 24-26 showed the pressure drop in the stenotic region along x-axis. The values for the pressure drop are negative which implied a rise in pressure in the stenotic region as x increased for all values of δ. Also, the converging artery has highest pressure rise in the stenotic region comparing with diverging artery. Figure 27 depicts the streamline profiles for different values of ξ (non tapered, convergence and divergence) for comparison in the flow patterns.

5. Conclusion

A mathematical model for the effects of heat and mass transfer in a micropolar fluid flow in stenotic tapered artery has been analysed. The results have been studied for the case of mild stenosis and the following major findings are obtained.
(i) Temperature is higher in converging artery than diverging artery.
(ii) Concentration is lower in converging artery than diverging artery.
(iii) Brickmann number B_r increases the temperature and decreases the concentration.
(iv) Micropolar spin parameter and coupling number increase the temperature.
(v) Micropolar parameter and coupling number decrease the concentration.
(vi) As Soret number increases, concentration decreases.
(vii) Pressure rise in a stenotic region for all value of x.
(viii) As Sr and Br numbers increase, there is an increase in Sherwood number.

Steady blood flow is applicable to the capillary bed which is being controlled by an auto regulation there by making the organ to maintain constant flow rate. However, flow in artery may be char-

acterized as time dependent. Hence, future studies and challenges could be focused on unsteady blood flow in a micropoloar fluid.

REFERENCES

Abubakar, J.U. and Adeoye, A.D. (2020). Effect of radiative heat and magnetic field on blood flow in an inclined tapered stenosed artery, Int. Journal of Taibah University for Science, Vol. 14, pp. 77-86.

Agarwal, R.S. and Dhanapal, C. (1987). Numerical solution to the flow of micropolar fluid between porous wall of different permeability, Int. J. Engineering Science, Vol. 25, pp. 325-336.

Akbar, N.S. and Nadeem, S. (2010). Simulation of heat and chemical reactions on Reiner Rivlin fluid model for blood flow through a tapered artery with a stenosis, Heat and Mass Transfer, Vol. 46, pp. 531-539.

Ariman, T., Turk, M.A. and Sylvester, N.D. (1974). Appreciation of microcontinum fluid mechanics, Int. J. Engineering Science, Vol. 12, pp. 273-293.

Arun, K.M. (2017). Mathematical modelling of blood flow under artherosclerotic condition, American Journal of Applied Mathematics, Vol. 4, No. 6, pp. 324-329.

Arunkumar, M. (2015). Casson flow of blood through an arterial tube with overlapping stenoses, IOSR Journal of Mathematics, Vol. 11, No. 6, pp. 26-31.

Bhuvana, R., Maruthi K. and Umadevi C. (2016). A mathematical model for micropolar fluid flow through an artery with the effect of stenosis and post stenotic dilation, Applications and Applied Mathematical Int. J., Vol. 11, No. 2, pp. 680-692.

Charakaravaty, S. and Sen, S. (2005). Dynamic response of heat and mass transfer in blood flow through stenosed bifurcated arteries, Kore-Aust Rheology J., Vol. 17, pp. 47-62.

Charm, S., Paltiel, B. and Kurland, G.S. (1968). Heat transfer coefficient in blood flow Biorhelogy, Biorheology J. , Vol. 5, No. 2, pp. 133-145.

Chinyoka, T. and Makinde, O.D. (2014) Computation dynamics of arterial blood flow in the presence of magnetic field and thermal radiation therapy, Advance in Mathematical Physics, Vol. 2014, Article ID 915640, pp. 1-9.

Eringen, A.C. (1966). Theory of micropolar fluid, Mech. J. Math, Vol. 16, pp. 1-18.

Gregorz Lukaseicz (1999), *Fluid Theory and Application* (First Edition), Birkhauser Boston.

Khs Mekheimer and Elkot, M.A. (2008). The micropolar fluid model for blood flow through a tapered artery with stenosis, Acta Mech. Sin., Vol. 24, pp. 637-644.

Kolios, M.C., Sherar, M.D. and Hunt, I.W. (1995). Large blood vessel colling in heated tissues a numerical study, Physics in Medicine and Biology J., Vol. 40, pp. 477 - 484.

Kumar, R.S. (2015). The effect of the couple stress fluid flow on MHD peristaltic motion with uniform porous medium in the presence of slip effect, Jordan Journal of Mechanical and Industrial Engineering, Vol. 9, No. 6, pp. 269 - 278.

Makinde, O.D., Khan, Z.H., Khan, W.A. and Tshehla, M.S. (2017). Mageto hemodynamics of nanofluid with heat and mass transfer in a slowly varying symmetrical channel, International Journal of Engineering Research in Africa, Vol. 28, pp. 118-141.

Mann, F.G., R., Essex, H. and Blades, E.J (1938). Effect of blood flow on decreasing the lumen of a blood vessel, Sugery, Vol. 4, pp. 4249-4252.

Mir Golam, R., Abdur Razzak and Mamum, M. (2013). Pulsatile non Newtonian blood flow through a model of Arterial stenosis, Procedia Eng J., Vol. 56, 225-231.

Nadeem, S., Akbar, N.S. and Hayat, T. (2011), Influence of heat and mass transfer on Newtonian bio magnetic fluid of blood flow through a tapered porous arteries with a stenosis, Springer Science Business Media, Vol. 91, pp. 81-100.

Neelam, S. (2016). Mathematical analysis of blood flow through with mild stenosis, International Journal of Computing Science and Mathematical, Vol. 17, pp.103-109.

Ogulu, A. and Abbey, T.M. (2005). Simulation of heat transfer on a oscillatory blood flow in an indented porous artery, Int. Communications in Heat and Mass Transfer, Vol. 32, pp. 983-985.

Om Prakash, Makinde, O.D., Singh, S.P,, Jain, N. and Kumar, D. (2015). Effect of Stenosis on non Newtonian flow of blood in blood vessels, International Journal of Bio Mathematics, Vol. 8, No. 1, pp. 1-13.

Philip, D. and Chandra, P. (1995). Peristaltic transport of simple micropolar fluid, Proc. Natl. Acad. Sci. Indian, Vol. 65A, pp. 65-74.

Prakash, J., Makinde, O.D. and Ogulu, A. (2004). Magnetic effect on oscillatory blood flow in a constricted tube, Botswana Journal of Technology, Vol. 13, No. 1, pp. 65-74.

Ranama, J.V. and Srikamath, D. (2015). The polar fluid model for blood flow through a tapered artery with overlapping stenosis, effect of catheter and velocity slip, Applied Bionics and Bio mechanics Article, pp. 1-2. http://dx.doi.org/11.55/2015/174387

Sanjeev, K. and Diwakar, C. (2013). Blood flow resistance for a small artery with the effect of multiple stenosis and post stenotic dilation, Int. J. Eng. Sci Emerging Technologies, Vol. 6, No. 1, pp. 57-64.

Srinivasacharya, D. and Madhavarao, G. (2016). Computational analysis of magnetic field influence on pulsatile flow of couple stress fluid through a bifurcated artery, Computer Methods and Programs in Biomedicine, Vol. 137, pp. 269 - 279.

Srivastava, L.M. (1985). Flow of couple stress through stenotic blood vessel, J. of Biomechanics, Vol. 18, pp. 479-485.

Young, D.F. (1968). Effect of time dependent stenosis of flow through a tube, J. Eng., Vol. 90, pp. 248-254.

Appendix

Salient flow properties are displayed in Figures 3-27.

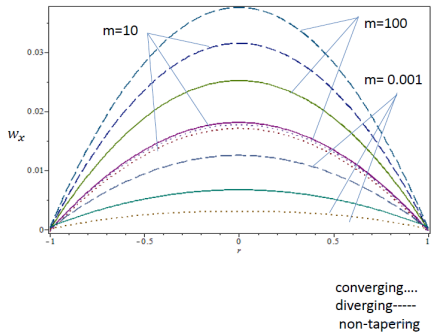

Figure 3. Graph of the axial velocity w_x against r at $N = 0.8$, $K_1 = 0.2$, $n = 2$ and $\delta = 0.2$ for variation of m

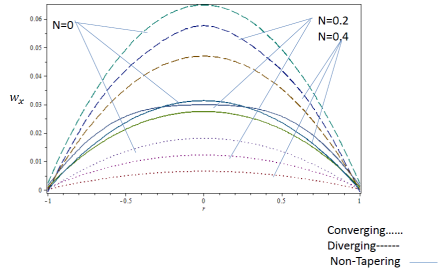

Figure 4. Graph of axial velocity w_x against r at $m = 5$, $n = 2$, $\delta = 0.2$ and $m = 5$ for variation of N

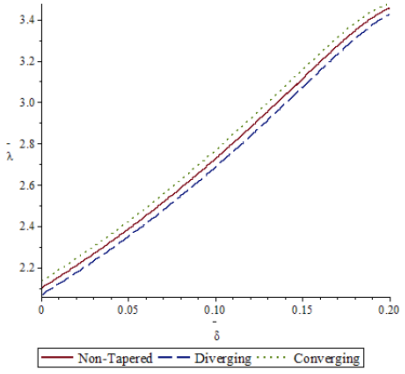

Figure 5. Graph of dimensionless resistance to flow λ, against δ at $N = 0.8$, $m = 5$, and $n = 2$ varying ξ

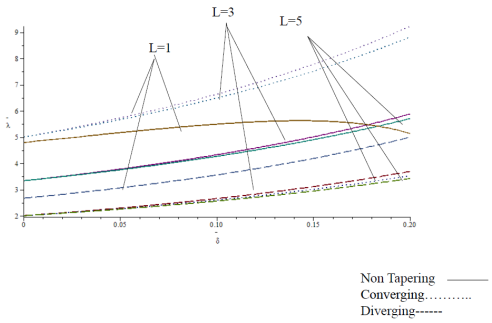

Figure 6. Graph of dimensionless resistance to flow λ, against δ at $N = 0.8$, $m = 5$ and $n = 2$ varying L

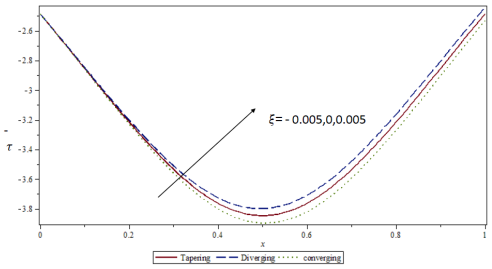

Figure 7. Graph of dimensionless wall shear stress τ against x at $N = 0.8$, $L = 1$ and $\delta = 0.2$ varying ξ

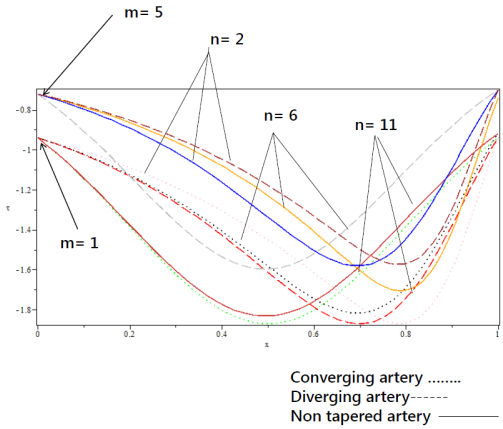

Figure 8. Graph of dimensionless wall shear stress τ against x for $L = 1$ and $\delta = 0.2$ varying m and N

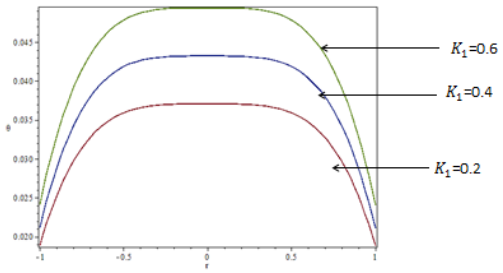

Figure 9. Graph of temperature against r at $m = 5$, $Br = 0.83$, $n = 2$, and $\delta = 0.2$ for different values of K_1

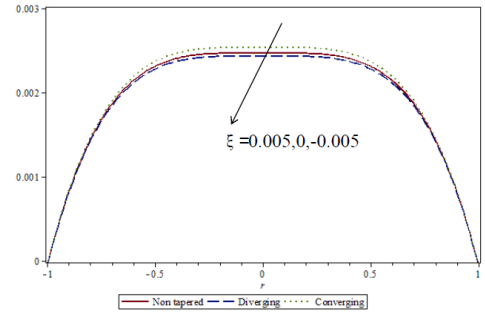

Figure 10. Graph of temperature against r at $m = 5$,$Br = 0.83$, $n = 2$, $K_1 = 0.2$ and $\delta = 0.2$ varying ξ

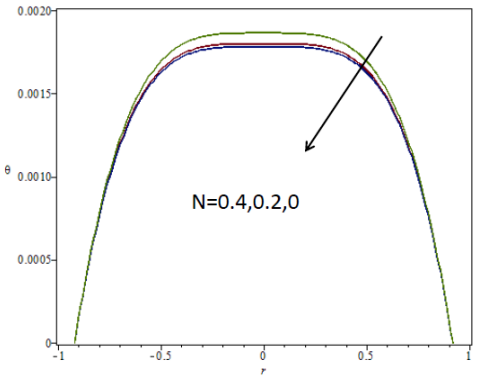

Figure 11. Graph of temperature against r at $N = 0.6$, $Br = 0.83$, $K_1 = 0.2$, $n = 2$, ξ and $\delta = 0.2$ varying N

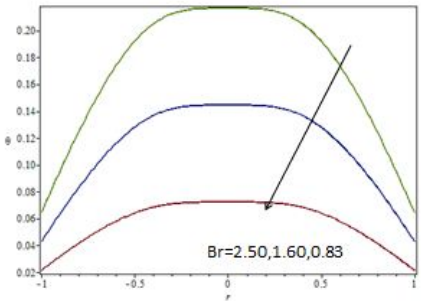

Figure 12. Graph of temperature against r at $N = 0.6$, $\xi = 0$, $K_1 = 0.2$, $n = 2$, and $\delta = 0.2$ for variation of Br

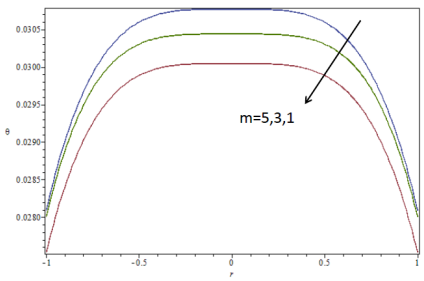

Figure 13. Graph of temperature against r at $N = 0.6$, $Br = 0.83$, $K_1 = 0.2$, $n = 2$, and $\delta = 0.2$ varying m

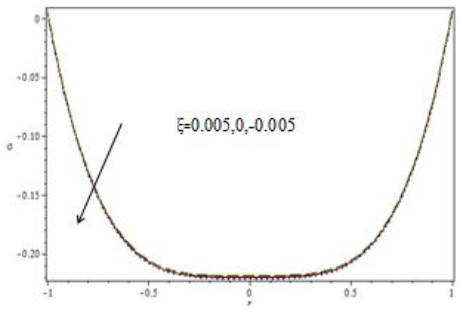

Figure 14. Graph of concentration against r at $m = 5$, $n = 2$, $Br = 0.83$, $K_1 = 0.2$, and $\delta = 0.2$ varying ξ

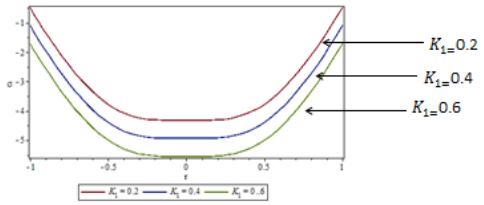

Figure 15. Graph of concentration against r at $m = 5$, $n = 2$, $Br = 0.83$, $\xi = 0$, and $\delta = 0.2$ varying K_1

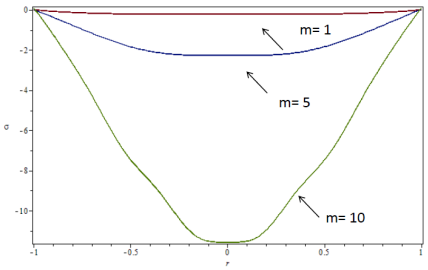

Figure 16. Graph of concentration against r at $N = 0.8$, $Br = 0.83$, $K_1 = 0.2$, $n = 2$, and $\delta = 0.2$ varying m

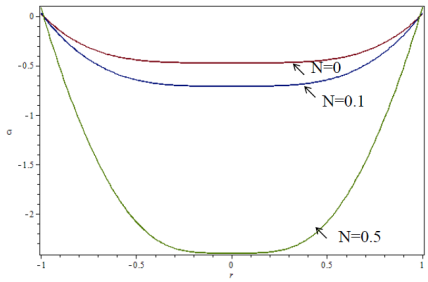

Figure 17. Graph of concentration against r at $Br = 0.83$, $K_1 = 0.2$, $n = 2$, $\delta = 0.2$, and $m = 5$, varying N

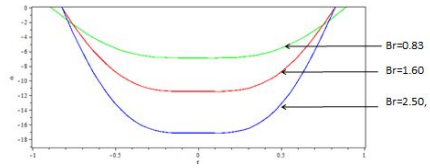

Figure 18. Graph of concentration against r at $m = 5$, $K_1 = 0.2$, $N = 0.8$, $n = 2$, and $\delta = 0.2$ varying Br

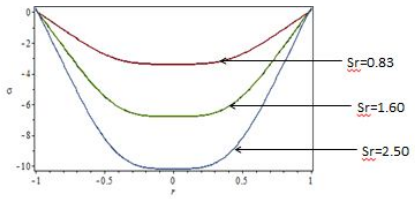

Figure 19. Graph of concentration against r at $m = 5$, $K_1 = 0.2$, $Br = 0.83$, $n = 2$, and $\delta = 0.2$ varying Sr

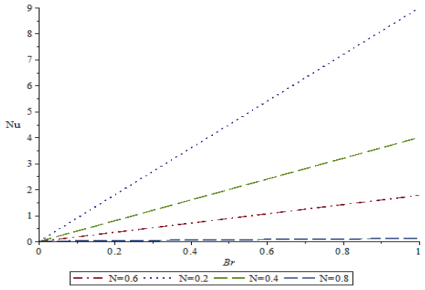

Figure 20. Graph of Nusselt number Nu against Br at $m = 5$, $K_1 = 0.2$, $n = 2$, and $\delta = 0.2$ varying N

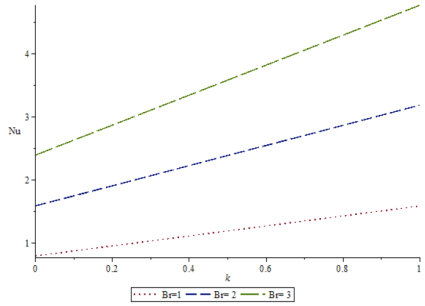

Figure 21. Graph of Nusselt number Nu against K at $m = 5$, $K_1 = 0.4$, $n = 2$, and $\delta = 0.2$ varying Br

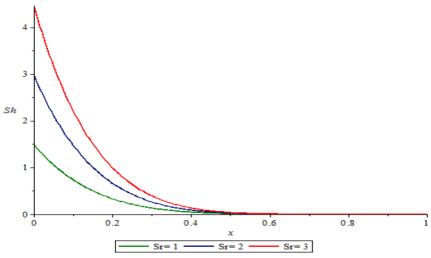

Figure 22. Graph of Sherwood number Sh against x at $m = 5$, $K_1 = 0.4$, $n = 2$, and $\delta = 0.2$ varying Sr

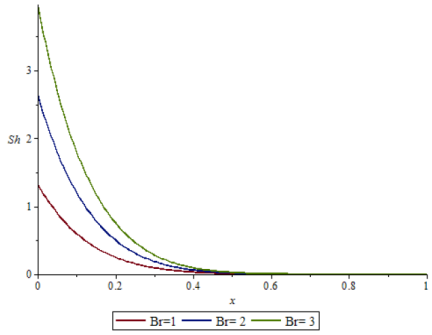

Figure 23. Graph of Sherwood number Sh against x at $m = 5$, $K_1 = 0.2$, $\delta = 0.2$ varying Br

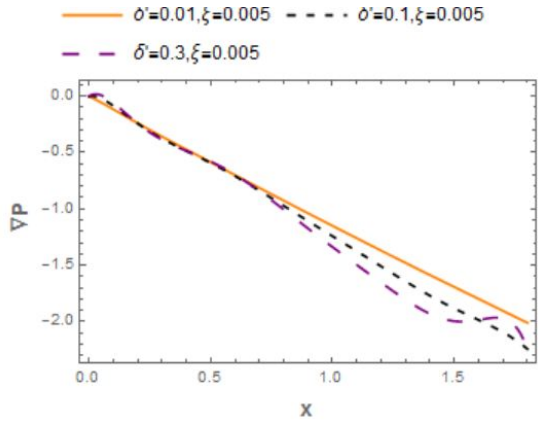

Figure 24. Graph of pressure drop against x at $m = 5$, $n = 2$, $N = 0.4$ and $\xi = 0.005$ varying δ

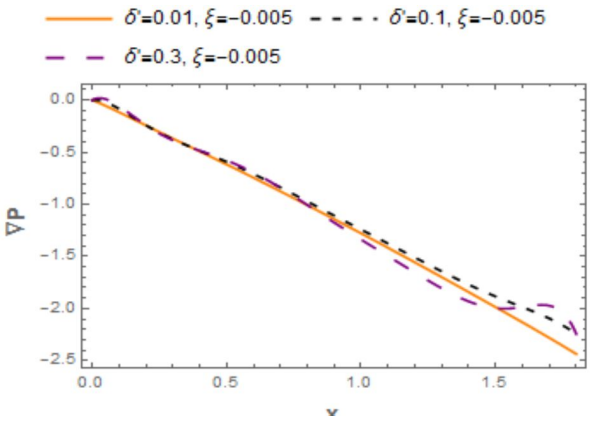

Figure 25. Graph of pressure drop against x at $m = 5$, $n = 2$, $N = 0.4$ and $\xi = -0.05$ varying δ

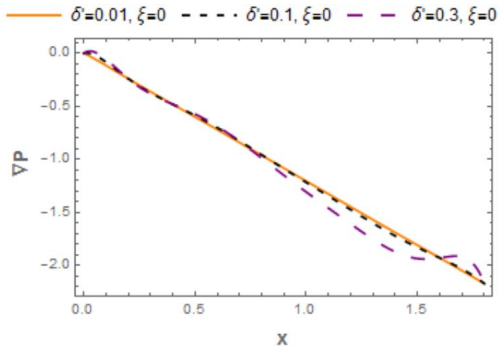

Figure 26. Graph of pressure drop along x axis $m = 5$, $n = 2$, $N = 0.4$ and $\xi = 0$ varying δ

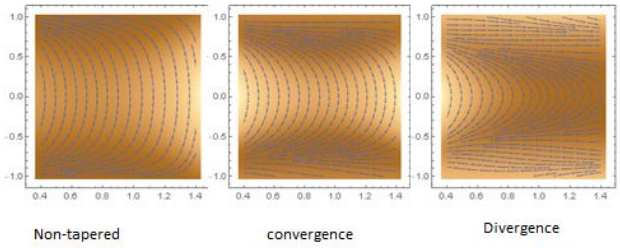

Figure 27. Graph of streamlines at the stenotic region for $m = 5$, $n = 2$, $N = 0.4$, $\xi = 0$, $\xi = 0.05$ and $\xi = -0.05$